Faraday Discussions

PAPER

Operando study of palladium nanoparticles inside UiO-67 MOF for catalytic hydrogenation of hydrocarbons

A. L. Bugaev,*[a,b] Alexander A. Guda,[a] Kirill A. Lomachenko,[c] Elizaveta G. Kamyshova,[a] Mikhail A. Soldatov,[a] Gurpreet Kaur,[d] Sigurd Øien-Ødegaard,[d] Luca Braglia,[a,b,e] Andrea Lazzarini,[d] Maela Manzoli,[e] Silvia Bordiga,[b,d] Unni Olsbye,[d] Karl P. Lillerud,[d] Alexander V. Soldatov,[a] Carlo Lamberti*[a,g]

Functionalization of metal-organic frameworks with metal nanoparticles (NPs) is a promising way for producing advanced materials for catalytic applications. We present synthesis and in situ characterization of palladium NPs encapsulated inside functionalized UiO-67 metal-organic framework. The initial structure was synthesized with 10% of PdCl2bpydc moieties with grafted Pd ions replacing standard 4,4'-biphenyldicarboxylate linkers. This material exhibits the same high crystallinity and thermal stability of standard UiO-67. Formation of palladium NPs was initiated by sample activation in hydrogen and monitored by in situ X-ray powder diffraction and X-ray absorption spectroscopy (XAS). The reduction of PdII ions to Pd0 occurs above 200 °C in 6% H2/He flow. The formed palladium NPs have the average size of 2.1 nm as limited by the cavities of UiO-67 structure. The resulting material showed high activity towards ethylene hydrogenation. In reaction conditions, palladium was found to form carbide structure indicated by operando XAS, while formation of ethane was monitored by mass spectroscopy and infra-red spectroscopy.

Received 22th December 2017, Accepted 00th January 2018

DOI: 10.1039/x0xx00000x

www.rsc.org/

[a] *The Smart Materials Research Center, Southern Federal University, Sladkova 178/24, 344090, Rostov-on-Don, Russia Email: abugaev@sfedu.ru*

[b] *Department of Chemistry and NIS Interdepartmental Centre, University of Turin, via P. Giuria 7, 10125 Turin, Italy*

[c] *European Synchrotron Radiation Facility, 71 avenue des Martyrs, CS 40220, 38043 Grenoble Cedex 9, France † Footnotes relating to the title and/or authors should appear here.*

[d] *Centre for Materials Science and Nanotechnology, Department of Chemistry, University of Oslo, Sem Saelands vei 26, 0315 Oslo, Norway*

[e] *CNR-IOM, TASC Laboratory, in Area Science Park, S.S.14, Km 163.5, I-34149, Trieste, Italy*

[f] *Department of Drug Science and Technology, University of Turin, via Pietro Giuria, 10125 Turin, Italy*

[g] *Department of Physics and CrisDi Interdepartmental Centre, University of Turin, via P. Giuria 1, 10125 Turin, Italy Email: carlo.lamberti@unito.it*

† Electronic Supplementary Information (ESI) available [electron diffraction analysis; cif file of the XRPD refinement]. See DOI: 10.1039/x0xx00000x

1. Introduction

In the last twenty years, the synthesis of new types of metal organic framework (MOFs) raised exponentially.[1-18] Additional degree of freedom comes from the functionalization of MOF materials[19-23 24-35] that allows obtaining new structures, with specifically targeted functionalities. Among the many classes of MOFs, the UiO-66/67/68 family[17, 34, 36-45] exhibits a remarkable thermal and chemical stability. The UiO-66/67/68 frameworks are obtained by connecting the 12-fold coordinated $Zr_6O_4(OH)_4$ inorganic cuboctahedron with organic linkers of increasing length 1,4-benzene-dicarboxylate, (bdc), 4,4'-biphenyl-dicarboxylate (bpdc) or 4,4'-terphenyl-dicarboxylate (tpdc) respectively.[36] Due to their outstanding stability, UiO-66/67/68 MOFs and related functionalized versions, have been attractive candidates for a large number of applications in the fields of catalysis,[46-59] photocatalysis,[46, 60] H_2,[38] CH_4,[61, 62] CO_2,[57, 63-65] H_2O[65] and CH_3OH[65] uptake, proton conduction,[66, 67] removal of air[68] and water[69] contaminants, gas separation,[70-72] sensor applications,[73] and for radioactive waste scavenging.[74]

The use of bpdc instead of bdc ligand, in the synthesis of UiO-67, results in symmetric expansion of UiO-66 topology (Figure 1a,b). The inorganic cornerstone in the structure is still 12-coordinated $Zr_6O_4(OH)_4(CO_2)_{12}$ cluster that gives high temperature stability to both UiO-66 and UiO-67 frameworks, as determined by thermogravimetric analysis (TGA), see Figure 1c. The longer linker implies that both the tetrahedral and octahedral microporous cages are of wider dimension in the UiO-67 case (Figure 1ab), moving from 7.5 to 12 Å and from 12 to 16 Å, respectively. This implies an increased pore volume with respect to UiO-66, as quantified by the N_2 adsorption isotherms, see Figure 1d. They are of Type Ib, indicating a perfectly microporous material possessing a very narrow pore size distribution. The shape of the N_2 isotherms is the same reported for UiO-66, with the plateau shifted to higher adsorbed volume. Accordingly, the UiO-67 surface area (S_{BET} = 1877 $m^2\ g^{-1}$) and micropore volume (V_{micro} = 0.85 $cm^3\ g^{-1}$) are more than the double than those of UiO-66 (S_{BET} = 850 $m^2\ g^{-1}$ and V_{micro} = 0.43 $cm^3\ g^{-1}$), as expected.

Also for the UiO-66/67/68 class of MOFs, different functionalization strategies were employed to enhance the material properties. Among others, we mention: functionalization by insertion of other metals in the inorganic cornerstone $M_xZr_{6-x}O_4(OH)_4$ (M = Hf, Ce, Ti);[49, 59, 65, 74, 75] functionalization by controlled defect engineering (missing linkers, metal centres or inorganic cornerstones);[17, 34, 39-43, 47, 63, 76-78] bromo-, nitro-, and naphthalene-functionalization of UiO-66/67;[79-82] proline-functionalization of UiO-67/68[83]; functionalization by use of biphenyl-, terphenyl-, and quaterphenyl-based linkers;[84] N-quaternization of the pyridine sites of UiO-67.[64]

With this respect, there are multiple choices of relatively easy ways to functionalize the linker of the UiO-67 with metal sites by substituting a fraction of the standard bpdc linkers with bipyridine-dicarboxylate (bpydc) linker, as described in the experimental section. In such way, Fe(II),[85] Ni(II),[86] Cu(II),[53, 87, 88] Ru(II),[46] Rh(III),[89, 90] Ir(III),[46, 90] Re(I),[46] Pt(II),[60, 88, 91-93] Pt(IV), [60, 88, 91, 92] and Pd(II),[48, 94] have already been successfully grafted to the two N atoms of the functionalized bpydc linker of UiO-67 MOFs. Recent works found particularly interesting the functionalization of UiO-67 with $PdCl_2$ bpydc. Fei et al.[48] showed that the atomically isolated Pd^{II} species, grafted to the UiO-67 framework via the bpydc linker exhibit efficient and recyclable catalytic activity for the Suzuki-

Miyaura cross-coupling reaction. Chen et al.[94] showed that Pd NPs hosted inside the UiO-67 pores exhibit a high selectivity in the hydrogenation of styrene even at room temperature and atmospheric H_2 pressure.

In this work we show that we succeeded in the synthesis of UiO-67-Pd MOF via the pre-made linker synthesis (PMLS) functionalization approach,[91] as proven by thermogravimetric analysis (TGA) and, synchrotron-based X-ray powder diffraction (XRPD) and extended X-ray absorption spectroscopy (EXAFS) analyses. The formation of Pd NPs inside the pores of UiO-67 framework was followed by *operando* XRPD, EXAFS and X-ray absorption near edge structure (XANES) techniques. Finally, the conversion of ethylene into ethane was chosen as key hydrogenation reaction and was followed by *operando* EXAFS/XANES and IR spectroscopies. Comparison with previous studies on Pd/C catalyst with slightly larger average particle size (2.6 vs. 2.1 nm) allowed us to demonstrate the size-dependent effects in the formation of palladium hydride and carbide phases under reaction conditions.

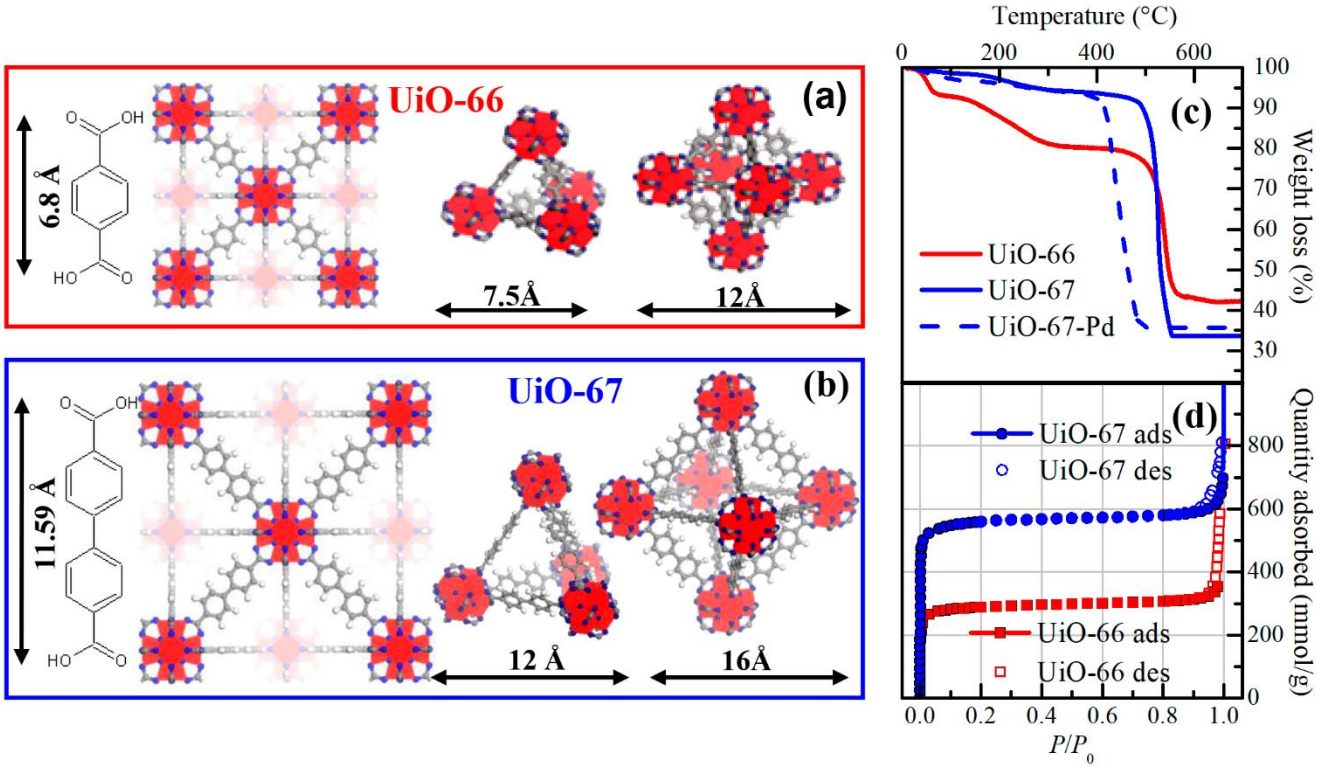

Figure 1. Structure of UiO-66 (a) and UiO-67 (b) MOFs with corresponding linker length and pore sizes. Part (c): TGA curves for UiO-66 (red) and UiO-67 material without (solid blue curve) and with 10% $PdCl_2$bpydc functionalisation (dashed blue curve). Part (d): volumetric N_2 adsorption isotherms recorded at 77 K on UiO-66 (red squares) and UiO-67 (blue circles). Empty and filled scatters refer to the adsorption and desorption branches, respectively. Adapted with permission from Chavan et al 2012,[38] copyright RSC 2012.

2. Experimental and methods

2.1. Synthesis and TGA characterization

The investigated UiO-67-Pd MOF has been prepared with the PMLS functionalization approach.[91] as described in the following. DMF and demineralized H_2O were added to a 250 mL Erlenmeyer flask with a magnetic stirring bar. $ZrCl_4$ was slowly added to the solution, and completely dissolved. The slow addition was found to be particularly important, as it reacts exothermically with water. Afterwards, benzoic acid, which is used as modulator,[95] was added and dissolved rapidly. The flask was then heated up to 110 °C while stirring. bpdc and $PdCl_2$bpydc were added simultaneously in a 10:1 molar ratio and gradually over a period of about 30 seconds. A clear solution was obtained shortly after the addition. Afterwards, the stirring bar was removed and the flask was placed in an oven at 120 °C for two days. The solvent was removed using vacuum filtration and the residual slurry was placed back into the flask. About 50 mL of DMF was added to the flask together with a stirring bar. The mixture was then stirred overnight to remove residual modulator (benzoic acid) at 40 °C and filtered afterwards. 50 mL of THF was then added, and the mixture was stirred for two to three hours. THF was removed using a vacuum filtration setup and an extra 30 mL of THF was used to wash the powder on the filter. After filtrating, the powder was collected in an uncovered glass vial and put in an oven at 60 °C overnight to remove THF. The following day the temperature was increased to 200 °C to remove any residual high boiling point species, and the powder was recovered after drying overnight.

TGA analysis was performed on a STA 449 Fx - Jupiter instrument, by flowing a mixture of 5mL/min O_2 and 20mL/min of N_2 and using a ramp rate of 5°C/min. 20 mg of non-functionalized UiO-67, and functionalized by 10% $PdCl_2$bpydc were weighted and transferred into an Al_2O_3 sample-holder. It has to be noted that the samples were not activated again (before the TGA measurement), to observe the effect of atmospheric adsorbate on the MOF.

2.2. *In situ* and *operando* XAS and XRPD measurements

Almost simultaneous XRPD and Pd K-edge XAS data were collected at the BM31[96, 97] of the ESRF (Grenoble, France), proposal #MA2930. The beamline allows fast (about 30 s) switching between XRPD and XAS setups, allowing measuring under each of reaction conditions (temperature and gas composition) both XRPD and XAS data.[98-100] The sample was loaded inside a 1.5 mm quartz glass capillary and fixed with quartz wool from both sides. The mass of the sample was 10 mg. The capillary was glued into a metal holder connected with a gas line equipped with remotely controlled mass flow controllers and electric valves. The composition of the gas outlet from the capillary was controlled by means of Pfeiffer Omnistar mass spectrometer. A gas blower was positioned below the sample to control the temperature. *In situ* H_2-temperature programmed reduction (TPR) was performed following a heating ramp of 5 °C min^{-1} in a flow of 6% H_2 in He (total flow 50 ml·min^{-1}), and followed by XRPD and XAS data collection.

XAS spectra at Pd *K*-edge were obtained in the transmission mode using a continuous scanning regime of the double crystal Si(111) monochromator in the energy range from 24.1 to 25.0 keV which took approximately 10 minutes per spectrum. Pd foil was measured simultaneously with

each spectrum for energy calibration using a third ionization chamber.[101] The spectrum of the sample after activation was analysed within first-shell Fourier approach using Demeter 0.9.21 package.[102] Real space data fitting in the *R*-range from 1.0 to 3.1 Å was performed on the Fourier-transformed k^2-weighted data in the *k*-range from 3.0 to 11.0 $Å^{-1}$. The amplitude reduction factor $S_0^2 = 0.74 \pm 0.04$ was obtained by fitting the spectrum of palladium foil, and fixed at this value for the nanoparticles, which allowed us to determine the corresponding Pd coordination number (*N*). To resolve the correlation between *N* and Debye-Waller parameter (σ^2), $\sigma^2(N)$ dependencies were obtained for *k*-weighting of 1, 2, and 3, and the corresponding *N* values were obtained as an intersection of the obtained $\sigma^2(N)$ curves for UiO-67-Pd sample after H_2-TPR.[103, 104] The evolution of Pd NPs formation was obtained by linear combination fit in the XANES region of the spectra. In addition, the spectra of as-prepared UiO-67-Pd material and reference $PdCl_2$bpydc compound were measured *ex situ* at BM23 beamline of ESRF in a pelletized form to obtain better signal to noise ratio. These spectra were fitted in the *R*-range from 1.11 to 2.33 Å on the Fourier-transformed k^3-weighted data in the *k*-range from 3.0 to 18.0 $Å^{-1}$.

XRPD was measured using λ = 0.51353(1) Å radiation, selected by a Si(111) channel-cut monochromator. CMOS-Dexela 2D detector covered the 2θ range from 2° to 32°. The values of λ, sample to detector distance and detector tilts were optimized by Rietveld refinement of NIST LaB_6 and Si samples and kept fixed in the refinement of UiO-67-Pd sample. For each experimental point, 20 diffraction images and 20 dark images (with the X-ray shutter closed) were collected. The Rietveld refinement of the initial material was performed in Jana2006 code.[105] In this work we report only weighted profile *R*-factor (R_{wp}) as a main criterion of fit quality, because correct estimation of the reduced χ^2 is complicated for the data collected with 2D detector, since pixels cannot be treated as Poisson counters. However, the fact that different statistics were accumulated in different 2θ-regions, due to the use of 2D detector, was taken into account for R_{wp} calculation.

2.3. Combined *operando* DRIFT-MS spectroscopy

IR spectra were collected using a Bruker Vertex 70 instrument, equipped with a liquid nitrogen-cooled MCT detector and a Harrick Praying Mantis DRIFT cell able to perform the measurements in the controlled atmosphere and temperature. For each spectrum, 128 scans with a resolution of 2 cm^{-1} were acquired. Mass spectra were collected with a Pfeiffer Omnistar GSD 301 O2 instrument, which was connected directly to the outlet of the DRIFT cell during the whole process, from activation till the end of the reaction. 25 mg of UiO-67-Pd was inserted in the DRIFT sample holder and activated from 25 °C to 300 °C with a 10 °C min^{-1} ramp rate in a flow of 6% H_2 in He (total flow: 50 ml·min^{-1}). The sample was then equilibrated for 30 min at 300 °C in order to allow the formation of Pd NPs; afterwards the gas flow was switched to pure He for 30 min at 300 °C to perform the removal of the fraction of hydrogen in the NPs in the form of PdH_x.[99, 106] The sample was then cooled to 25 °C in He to perform the reaction. Ethylene hydrogenation was performed at 4 different temperature steps: 25 °C, 40 °C, 60 °C and 80 °C with a total reactants flow of 50 ml min^{-1} (6% H_2, 6% C_2H_4, 88% He).

2.4. STEM measurements

High-resolution scanning transmission electron microscope (HR-STEM) images were obtained using a FEI Technai G2, F20 operated at 200 kV. The samples were dispersed in isopropanol prior to the analysis.

3. Results and discussion

3.1. Characterization of initial UiO-67-Pd material

Thermo-gravimetric analysis was performed for the pure UiO-67 and functionalized by $PdCl_2$bpydc (Figure 1c, blue solid and dashed curves, respectively). Both materials show a two-step weight loss corresponding to a typical MOF, where the first weight loss is for the loss of solvent and unreacted species and second weight loss is for the structural collapse of the MOF.[37, 38, 82, 93] The final weight loss after the complete degradation of the crystalline lattice of the material, results in a 35.6% of mass residue for the functionalized material and 33.6% of mass residue for the unfunctionalized one. This difference is due to the presence of palladium, which cannot be degraded and released during the measurement. Indeed, the difference in the mass% between the two samples fits perfectly with the amount of Pd present inside the sample structure. This quantitative agreement in the weight loss implies that the further Pd-functionalisation with Pd chloride did not leave the material with any retention of solvent or Pd-based linker. The stability of the functionalised sample is reduced after the grafting of $PdCl_2$ on the bpydc moieties, as testified by the lower temperature of decomposition (400°C against 550°C of the unfunctionalized material). However, we always operate in a safe regime since we never exceed the critical temperature: the H_2 reduction was performed up to 300 °C and ethylene hydrogenation reaction was performed below 100°C.

X-ray powder diffraction data (Figure 2) confirm that the starting material has UiO-67-like structure with *Fm*-3*m* symmetry and lattice parameter a = 26.7986(2) Å. Thus, Rietveld refinement was performed using the ideal UiO-67 structure for the starting parameters,[39] which already gave good agreement with experimental pattern (R_{wp} = 3.41). For the following step, we allowed to move C3 and C4 atoms of the linkers (see inset in the Figure 2) beyond their initial 96*j* crystallographic site with $x \neq z \neq 0$ and $y = 0$, to 192*l* site with $x \neq z \neq y \neq 0$, and to vary the occupancy of all atoms during refinement. This change provoked a decrease of R_{wp} to 3.22, giving in a linkers occupancy around 0.92 and slightly shifting C3 and C4 atoms perpendicularly to the initial plane of the aromatic rings. Then, due to the obtained shift of C3 and C4 atoms in y direction, we employed anisotropic displacement U_{ij} for C3 and C4 atoms using only diagonal ($i = j$) non-zero U_{ij} parameters and assuming $U_{11} = U_{33} \neq U_{22}$. This procedure further reduced R_{wp} to 3.18 yielding $U_{22} > U_{11}$ for both C3 and C4 atoms. Finally, we have added a Pd atom to 96*k* site, assuming that it is located equally in the $z = ½ - x$ plane, that goes perpendicularly to the aromatic rings plane, dividing the bpdc linker in the centre of C5–C5 bond. Similar to C3 and C4 atoms, we used anisotropic U_{ij} with $U_{11} = U_{33} \neq U_{22}$ and $U_{12} = U_{13} = U_{23} = 0$ also for Pd atom.

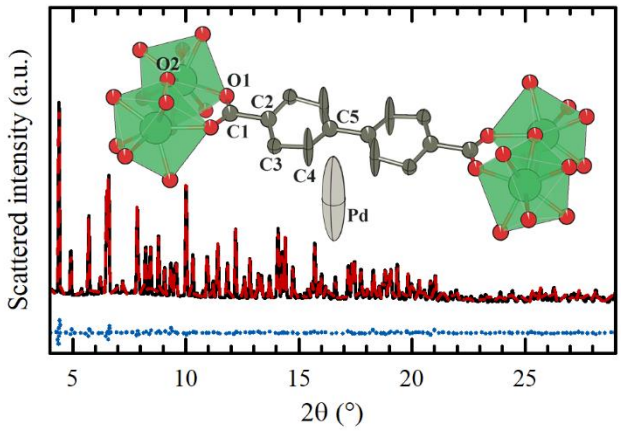

Figure 2. Experimental (solid black) and theoretical (dashed red) XRPD patterns with corresponding difference (dotted blue) of the initial UiO-67-Pd material, measured using 0.51353(1) Å radiation. The atomic structure represents a linker made of carbon atoms (dark grey) with palladium atom (grey) connecting the inorganic cornerstones of zirconium (green) and oxygen (red) highlighted by semi-transparent green polyhedra. The labels are reported for all inequivalent atoms. To illustrate the anisotropic displacement parameters for atoms C3, C4, and Pd atoms, the 50% probability ellipsoids are plotted. Cl atoms are not shown in this figure as they were not determined by XRPD, while N atoms occupy the same crystallographic position as C4 atoms and cannot be distinguished from them. Hydrogen atoms of aromatic rings are not shown because they cannot be detected by X-ray diffraction.

To reduce the number of parameters and increase the stability of the refinement we used common occupancy factor for all carbon atoms of the linkers. As the result, we obtained a stable and converging refinement with final R_{wp} = 3.16 and $U_{22} >> U_{11}$ for Pd and C4 atoms, while for C3 atoms $U_{22} \approx U_{11}$. The obtained occupancy for Pd atom was 0.091, which is close to the expected value, since 10% of the linkers contained a Pd atom. The addition of nitrogen atoms close to C4 atoms results in the unstable behaviour of the refinement procedure. This could be easily explained by general difficulties of powder diffraction technique to distinguish two atoms with similar scattering amplitudes at very close crystallographic positions. Therefore, big U_{33} parameters obtained for C4 atoms should account for the presence of nitrogen atoms, shifted from the ideal position of C4 atom in an ideal UiO-67 structure. Location of Cl atoms, which are expected to be bonded to Pd, was also not possible, probably, due to high thermal and structural disorder in their positions. This disorder can be qualitatively estimated by extrapolating the U_{33} values obtained for C4 and Pd atoms to the Cl one which should have even higher distance from the rotational axis of the linker. It should be noted, that the 2θ-range below 4.2° was intentionally excluded from the refinement as the intensities of the peaks in this region are affected by the beamstop, and cannot be used for Rietveld procedure. In addition, the exclusion of the low 2θ region allowed us to neglect the solvent during the refinement, as its presence affects only the intensity of the first strongest peaks.[107, 108] All structural parameters obtained by Rietveld refinement are reported in Table 1. The obtained occupancy and U_{ij} for Pd species indicate that they are close to detection limit of XRPD data. Thus, grafting of Pd atoms into UiO-67 structure was further explored by EXAFS data (vide infra).

Table 1. Atomic parameters obtained by the Rietveld refinement of the initial UiO-67-Pd material in the *Fm*-3*m* space group: fractional coordinates (*x*, *y*, *z*), isotropic (U_{iso}) or anisotropic (U_{ani}, values marked by *) atomic displacement parameters, occupancy factors, and site degeneration. The refined cell parameter is *a* = 26.79861(20) Å. The resulting R_{wp} parameter is 3.16. The values which were fixed or derived via other variables are underlined. For C3 and C4 atoms occupancy factor is twice lower than for C1, C2, and C5 atoms, as their shift from the initial symmetric position leads to artificial doubling of these atoms in the cell. For the atom labelling, see the inset in Figure 2.

atom	*x*	*y*	*z*	U_{iso} (Å^2)	Occupancy factor	site	*N* of atoms per unit cell
Zr	0.40773(8)	0	0.5	0.0095(8)	1.000	24e	24
O1	0.3671(2)	0	0.4270(2)	0.010(3)	0.960(13)	96j	92.16
O2	0.4539(2)	0.5 – *x*	1 – *x*	0.027(6)	0.96(3)	32f	30.72
C1	0.3839(4)	0	x	0.014(6)	0.947(9)	48h	45.46
C2	0.3404(5)	0	x	0.048(7)	0.947	48h	45.46
C5	0.2714(3)	0	x	0.043(6)	0.947	48h	45.46
C3	0.3564(5)	0.0147(10)	0.2933(4)	*0.039(12)	0.473	192l	90.82
C4	0.3192(4)	0.01(12)	0.2549(5)	*0.1(4)	0.473	192l	90.82
Pd	0.3155(15)	0.061(6)	0.5 – *x*	*0.69(17)	0.023(3)	96k	2.2

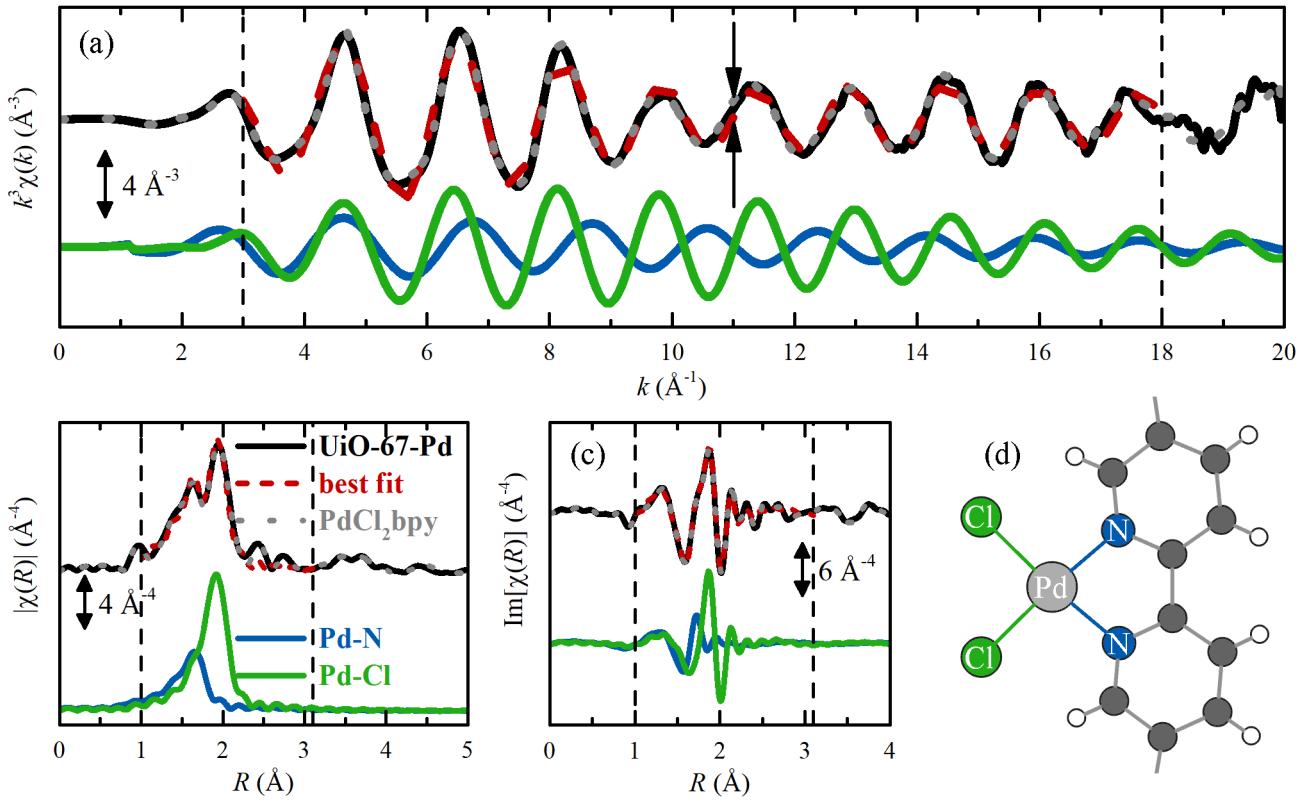

Figure 3. Summary of the EXAFS analysis performed on the spectra collected on samples in a pellet form reporting $k^3\chi(k)$ (a) and corresponding phase-uncorrected amplitude (b) and imaginary part (c) of the Fourier-transforms in *R*-space of experimental signal of UiO-67-Pd (black curves), best fit (red curves) with Pd–N (blue curves) and Pd–Cl (green curves) single scattering contributions, and experimental signal of $PdCl_2$bpydc model compound (grey curves). Vertical dashed lines define the intervals in *k*- and *R*-spaces used to perform the Fourier-transform and fit of the data respectively. Two vertical arrows in part (a) indicate the upper limit of the *k*-space used to fit the *in situ* EXAFS data collected on the sample placed in capillary. Part (d): graphical representation of the linker with $PdCl_2$. The quantitative results of the fit are reported in Table 2.

Table 2. Summary of the fits performed on the static EXAFS spectra collected at RT on the UiO-67-Pd MOFs and on the $PdCl_2$bpycd reference material. Δk = (3.0-18.0) $Å^{-1}$; ΔR = (1.11-2.33) Å. Underlined numbers refer to non-optimized parameters. The graphical quality of the fit, as well as the different contribution of the N and Cl ligands can be appreciated in Figure 3 (a) and (b-c) in *k*- and *R*-spaces, respectively.

Sample	Shell	*N*	*R* (Å)	σ^2 ($Å^2$)	E_0 (eV)	S_0^2
UiO-67-Pd	Pd–N	2	2.03 ± 0.01	0.0027 ± 0.0008	24359.7 ± 1.2	0.88 ± 0.7
	Pd–Cl	2	2.29 ± 0.01	0.0025 ± 0.0004		
$PdCl_2$bpycd	Pd–N	2	2.03 ± 0.01	0.0026 ± 0.0008	24359.8 ± 1.3	0.88 ± 0.8
	Pd–Cl	2	2.29 ± 0.01	0.0025 ± 0.0004		

Fourier-analysis of Pd *K*-edge EXAFS data was performed to determine precisely the local structure around palladium atoms and to prove the presence of chlorine atoms in the first coordination shell. *Ex situ* EXAFS data were collected on the sample prepared in the form of pellet having optimal thickness that allowed collecting high-quality data up to k = 18 $Å^{-1}$ shown in Figure 3a. For the as-prepared UiO-67-Pd material both XANES and EXAFS regions coincide with the ones of the reference $PdCl_2$bpycd linker. The Fourier-transform of the k^3-weighted data in the Δk range from 3 to 18 $Å^{-1}$ has a clear splitting of the first shell peak (Figure 3b) explained by Pd–Cl and Pd–N contributions with corresponding $R_{Pd\text{-}Cl}$ and $R_{Pd\text{-}N}$ of 2.288 ± 0.005 Å and 2.03 ± 0.01 Å, respectively. The Pd–Cl (green) and Pd–N (blue) contributions are reported in *k*- and *R*-spaces in parts (a) and (b-c) of Figure 3, respectively. The coordination numbers for both Cl and N atoms were fixed to 2. The combined XRPD/EXAFS study on the as prepared material testified that the functionalization procedure maintained the crystal structure of the UiO-67 framework and confirmed that Pd(II) centres are hosted in square planar geometry having two N framework atoms and two chlorines as first shell neighbours.

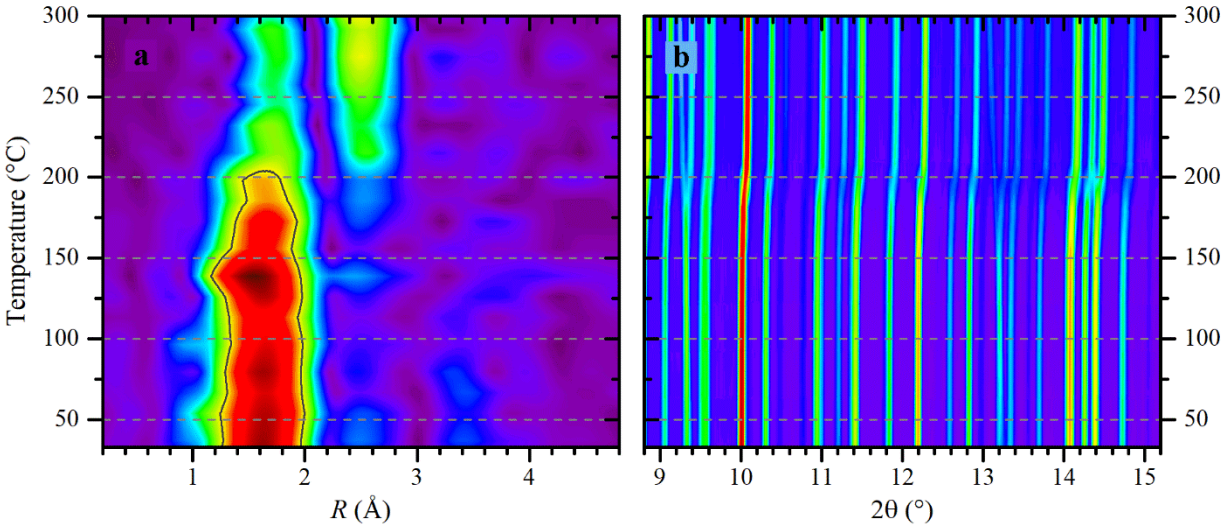

Figure 4. Evolution of (a) phase-uncorrected k^2-weighted Fourier-transformed EXAFS data in the 0.2 - 4.8 Å range and (b) XRPD patterns reported in the 9 – 15° 2θ-region during the H_2-TPR treatment of UiO-67-Pd in the 20 – 300 °C interval.

3.2. Formation of Pd NPs and evolution of UiO-67 structure monitored by combined *in situ* XAS and XRPD and *ex situ* STEM

The progressive formation of palladium NPs in UiO-67-Pd during H_2-TPR was monitored by *in situ* XAS and XRPD. The changes in the Fourier transform of EXAFS data indicate a decrease of the first peak at 1.6 Å (phase-uncorrected) which corresponds to Pd-N and Pd-Cl contributions, and formation of a new peak at 2.5 Å (phase-uncorrected) attributed to Pd-Pd contribution evidencing the nanoparticle formation (Figure 4a). Along all temperature scale XRPD data show that the UiO-67 structure is stable and preserves its initial crystallinity. At 200 °C, simultaneously with detachment of grafted Pd atoms from the linkers, observed in EXAFS, the Bragg peaks in XRPD patterns are shifting to higher 2θ angles (Figure 4b) which corresponds to a decrease of the cell parameter from 26.7986(2) to 26.730(2) Å.

At the same time, XANES spectra (Figure 5a) indicate a clear transformation of Pd^{II} features of $PdCl_2$bpydc to Pd^0 of Pd NPs. These changes were analysed by means of principal components analysis (PCA):[109-111] only two main components have been found and attributed to $PdCl_2$bpydc and Pd NPs (red and black spectra in Figure 5b, respectively). Figure 5c, reports the evolution of Pd NPs components along the H_2-TPR treatment (scattered squares). The full line in Figure 5c represents the best fit of the experimental points using the Boltzmann equation:

$$F(T, T_0, \tau) = 1 - \frac{1}{1+e^{(T-T_0)/\tau}} \qquad (1)$$

where the parameters T_0 and τ represent, respectively, the temperature when half of the palladium atoms are in Pd^0 state, and an estimation of the width of the temperature interval where the transition from Pd^{II} to Pd^0 occurs. Using Eq. (1), the fit of the experimental points obtained from the PCA analysis resulted in T_0 = 195 ± 2 °C and τ = 26 ± 2 °C.

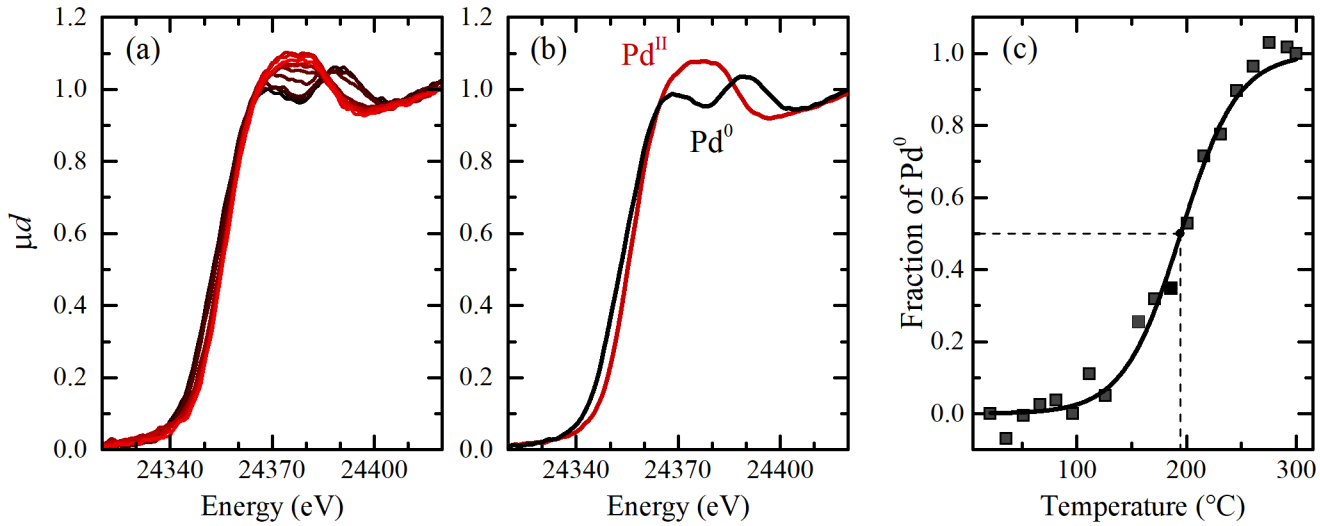

Figure 5. Part (a): evolution Pd *K*-edge XANES spectra during the H_2-TPR treatment of UiO-67-Pd in the 20 – 300 °C interval (from red to black). Part (b): main components, extracted from PCA analysis, from the series of XANES spectra collected, corresponding to $PdCl_2$bpydc (Pd^{II}, red curve) and Pd NPs (Pd^0, black curve) species. Part (c): Evolution of the Pd^0 component as a function of temperature obtained by PCA (black squares) and fitted by Boltzmann equation (black curve).

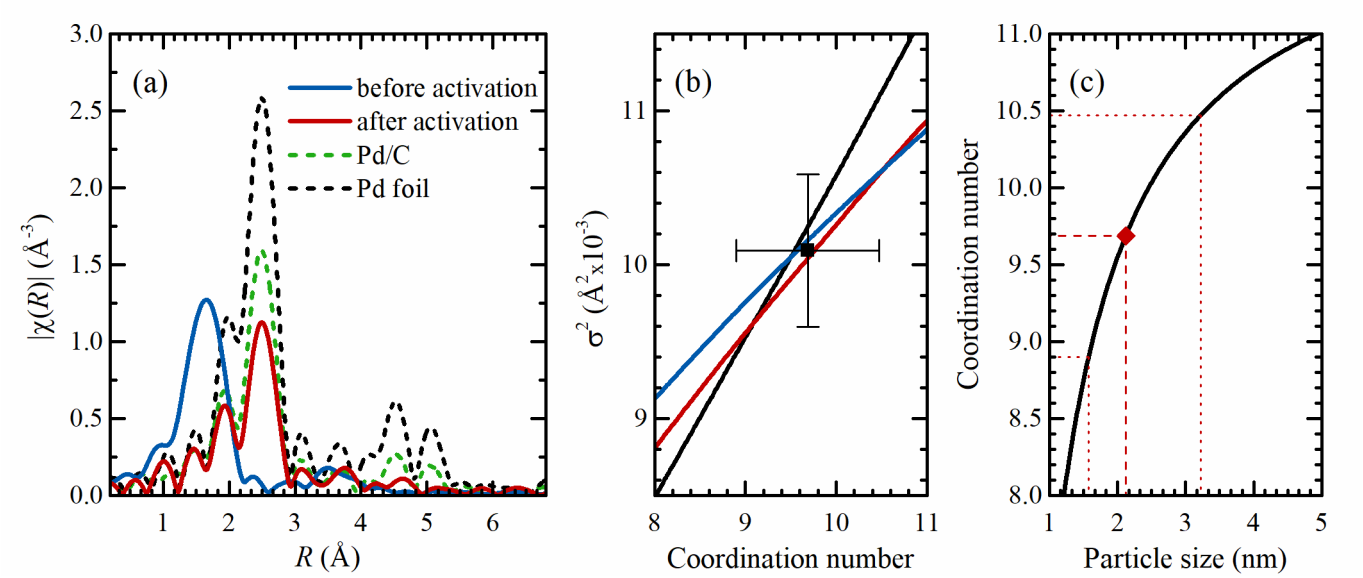

Figure 6. Part(a): Phase-uncorrected k^2-weighted Fourier-transformed EXAFS data of UiO-67-Pd before (blue curve) and after (red curve) activation compared to metallic palladium foil (black dashed curve) and supported Pd/C NPs[99] with average size 2.6 nm (green dashed curve). Part (b): $\sigma^2(N)$ dependencies obtained for k- (black), k^2- (red), and k^3- (blue) weighted data. The resulting σ^2 and N values obtained as an intersection region of these curves are shown with the black square with corresponding error bars. Part (c): Determination of the average nanoparticle size (red diamond, dashed curve) and its error limits (red dotted lines) according to the size equation.[113]

After activation in H_2, the sample was cooled down and the final EXAFS data were collected. The corresponding Fourier-transform of the obtained signal (Figure 6a, red curve) has much weaker amplitude of the Pd-Pd contribution at ~2.5 Å (phase-uncorrected) in comparison with FT of Pd foil (black dashed curve), and supported Pd/C NPs with average size of 2.6 nm,[99] used as a reference material, which indicates the formation of ultra-small palladium NPs. The Fourier analysis of EXAFS data showed a strong correlation between σ^2 and N parameters, resulting in different numerical results depending on the used k-weighting and k-interval. To resolve the correlation between σ^2 and N values, we have obtained $\sigma^2(N)$ dependencies by variation of coordination number using k-, k^2-, and k^3-weighted data. The intersection of the obtained curves (Figure 6b) was used to determine the final values of N = 9.7 ± 0.8 and σ^2 = 0.0101 ± 0.0005 Å^2. Then, using the correlation between the average first shell coordination number and the average NP diameter,[112-115] in assumption of the spherical shape of the particles, the particle size distribution is mainly comprised in the 1.6 – 3.2 nm interval, with an average value of 2.1 nm, note the asymmetric nature if this interval, as illustrated in Figure 6c. The fitted value of interatomic Pd-Pd distance R = 2.75 ± 0.01 Å is close to that of Pd foil. The high value of σ^2 = 0.0101 ± 0.0005 Å^2 in comparison with σ^2_{foil} = 0.0052 ± 0.0002 Å^2 is typical for the NPs due to the disordered structure of the subsurface region.

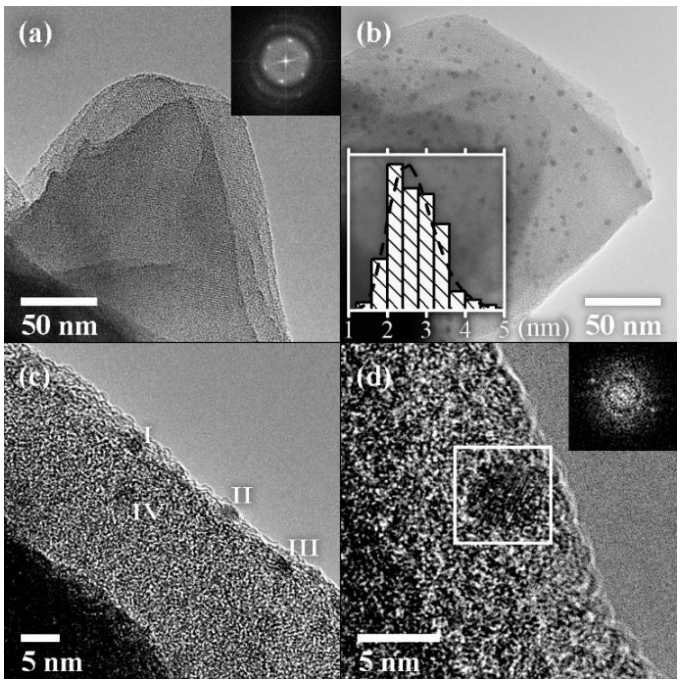

Figure 7. Representative STEM images of initial UiO-67-Pd material (a), and after H_2-TPR (b-d). Inset in part (a) shows the FT of the whole STEM image, inset in part (d) shows the FT of the area highlighted by white square. Inset in part (b) shows the particle size distribution. In part (c) four Pd NPs have been labelled as I, II, III and IV and are characterized by transversal sizes of 2.0 x 2.2, 2.0 x 2.5, 1.5 x 2.1 and 1.6x2.5 nm^2, respectively.

STEM images of the sample before and after H_2-TPR are shown in parts (a) and (b-c) of Figure 7, respectively (*ex situ* experiment). Remarkable is the resistance of the UiO-67 framework to the 200 keV electron beam, allowing observation of the interference fringes between two different crystallographic planes (main panels) as well as electron diffraction (insets). The analysis of electron diffraction (See Tables S1 and S2 of ESI) confirms that the observed reflections (Figure 7a) correspond to UiO-67 structure, in agreement with XRPD data reported in Section 3.1, and to (111) face of cubic Pd (JCPDS file number 00-001-1312). The low-magnification image reported in Figure 7b testifies that quite homogeneous distribution of Pd NPs over UiO-67 matrix is obtained after H_2-TPR. Figure 7c,d reports a selection of representative high-resolution STEM images. The inset in part (d) reports the electron diffraction pattern of the Pd NPs highlighted in the white box of the main part and confirms exposure of the. In part (c), four Pd NPs with size close to that determined by the EXAFS (2.1 nm, see Figure 6c) are evidenced with Roman labels from I to IV. The relatively low contrast between Pd NPs (Z = 46) and the UiO-67 matrix, containing a significant fraction of Zr atoms (Z = 40), complicates the detection of Pd NPs, particularly for the smallest ones.

According TEM results, the fraction of NPs with bigger sizes (right part of the size distribution curve) should be located not inside the UiO-67 pores, but on its surface. However, the low value of the averaged coordination number determined by EXAFS indicate that major fraction of the particles, complicated for TEM detection, should have sizes within 2 nm, and should fit the size of UiO-67 pores. Moreover, as evidenced by XRPD, formation of palladium NPs does not decrease the crystallinity of UiO-67.

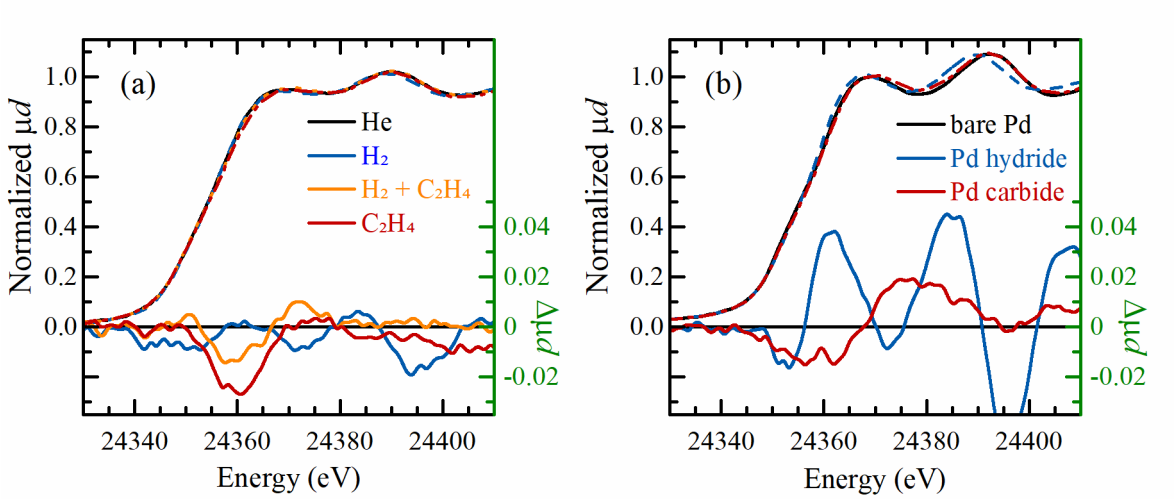

Figure 8. (a) XANES spectra of the activated sample after cooling down in He (black), exposed to H_2 (blue), in reaction conditions in a mixture of H_2+C_2H_4 (orange), and in C_2H_4 (red). The scale for the difference spectra is 10 times larger and is shown on the right axis (green). (b) XANES spectra for metallic (black), hydride (blue), and carbide (red) phases of Pd/C catalyst taken in similar conditions. Previously unpublished figure, reporting in part (b) data for 2.6 nm Pd NPs supported on carbon already published in Ref.[98]

3.3. Catalytic hydrogenation of ethylene: *operando* XANES and DRIFT experiments

Palladium is known to demonstrate high catalytic activity in hydrogenation of hydrocarbons, and to form Pd hydride and carbide phases in reaction conditions.[116] After the H_2-TPR experiment (Figure 4, Figure 5a), the sample was cooled down to 25 °C in He to maintain pure metallic state of the just-formed NPs (Figure 8a, black curve). Then, the sample was flushed with 20% H_2 in He at 25 °C (Figure 8a, dashed blue curve) to check if these NPs can form palladium hydride phase.[99, 106, 117] This procedure resulted in the increase of the Pd–Pd distances from $R_{Pd\text{-}Pd}$ = 2.75 ± 0.01 to $R_{Pd\text{-}Pd}$ = 2.78 ± 0.01 Å, as determined by Fourier analysis of EXAFS. This increase indicates formation of palladium hydride phase, however, the observed interatomic distances are smaller than R = 2.83 Å observed in similar conditions for Pd/C NPs with an average size distribution of 2.6 nm.[118] Thus, in the UiO-67-Pd sample the hydride phase is formed, but the amount of absorbed hydrogen is lower than in the case of the larger NPs supported on carbon. Indeed, the difference XANES spectra (Figure 8a, solid blue curve) have the same characteristic features of palladium hydride,[119] but they are much less pronounced than in difference XANES of 2.6 nm PdH_x particles (Figure 8b, solid blue curve) due to the lower concentration x in small PdH_x NPs inside UiO-67 framework.

IR spectroscopy[120-123] has been used to follow the hydrogenation of ethylene in *operando* conditions. Figure 9a shows the DRIFT spectra for the sample after activation (black curve) and during reaction at 25, 40, 60 and 80 °C (blue, green, orange, and red curves, respectively). The sample after activation does not present any noticeable differences with the non-functionalized UiO-67 system,[38, 124] since the insertion of the bipyridyl moieties gives rise to a signal which is in the same spectral region of the traditional linker, and since the Pd species (in the form of chlorides, hydrides and NPs) give rise to signals which are outside of our spectral window. Interesting are: (i) the absence of the modes of the dimethylformamide (DMF) molecule, in particular the band at 1690 cm^{-1},[123] reflecting the perfect desolvation of the material; (ii) the presence of the sharp band

at 3673 cm^{-1} due to μ_3(OH) group in the $Zr_6O_4(OH)_4$ cornerstone of the UiO-67 MOF,[37, 38] that resisted to the H_2-TPR treatment at 300 °C and that is almost unaffected during C_2H_4 hydrogenation (just redshifted by 2 cm^{-1}). The characteristic spectral features of the MOF framework are also maintained during reaction, due to the extremely mild conditions in which hydrogenation takes place (25-80 °C, 1 bar). The subtraction of the IR spectrum obtained on the UiO-67-Pd sample at 25 °C in He flow from that one obtained just after switching the gases to the reaction feed is reported as blue curve in the inset of Figure 9a and directly compared with that of gaseous ethylene and ethane (dark and light grey, respectively). After the He/(H_2 +C_2H_4 +He) feed switch, the formation of gaseous ethane (C–H stretching modes in the 3050-2850 cm^{-1} region) is almost instantaneously detected by both IR (Figure 9a, more evident in the inset) and MS (Figure 9b). The spectra reported in Figure 9a are also characterized by the almost total absence of spectral features belonging to gaseous ethylene, that should be visible in the 3200-3050 cm^{-1} region, see inset. The only clearly visible feature is the sharp band of the $\nu(CH_2)$ symmetric stretching mode of C_2H_4 with B_{3u} symmetry,[125] highlighted with the vertical dark grey segment. The IR features of ethylene are indeed more difficult to be detected in our experiment because of: (i) the fast conversion of C_2H_4 to C_2H_6; (ii) the higher extinction coefficients of the C–H stretching modes of ethane; (iii) the larger overlap of the C–H stretching modes of the UiO-67 linkers with that of C_2H_4. Figure 9b indicates that the C_2H_6 production slightly increases by a progressive temperature increase from 25 to 80 °C.

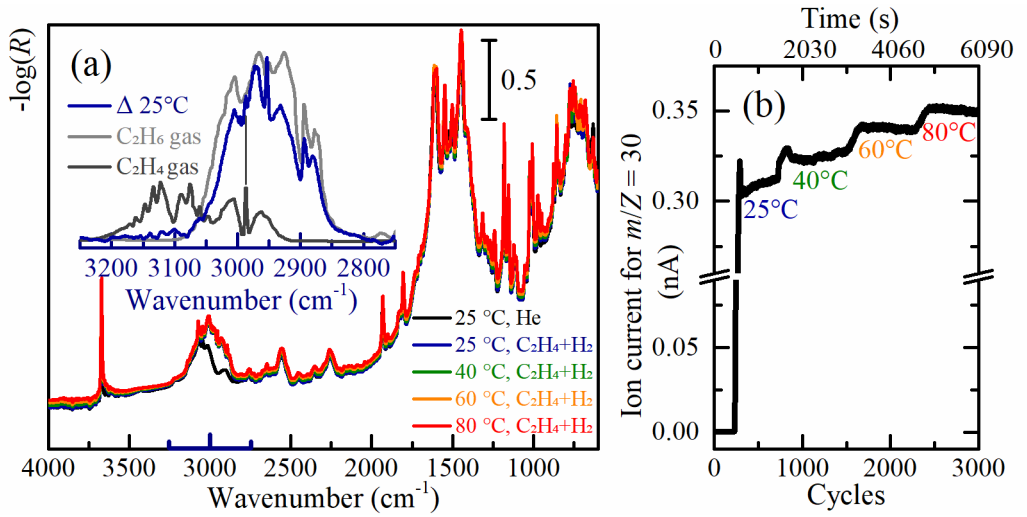

Figure 9. Part (a): DRIFT spectra of UiO-67-Pd at RT in He after reduction in H_2 (black spectrum) and during ethylene hydrogenation at 25, 40, 60 and 80 °C (blue, green, orange, and red curves, respectively). R = reflectance. Inset: magnification of the spectral region, from 3250 to 2750 cm^{-1}, involving the C–H stretching modes of the difference spectrum (blue – black), compared with the spectra of gaseous ethylene and ethane (dark and light grey, respectively). The vertical dark grey segment highlights the position of the sharp band of the $\nu(CH_2)$ symmetric stretching mode of C_2H_4 with B_{3u} symmetry.[125] Part (b): response of the MS reporting the *m/Z* ratio 30 of the ethane product along the *operando* DRIFT experiment. The He/(H_2 +C_2H_4 +He) switch occurred after 215 cycles (1 cycle = 2.03 s). The three temperature changes are accompanied by a sharp increase of the MS response.

4. Conclusions

We have performed a successful synthesis of UiO-67-Pd material with 10% of $PdCl_2$bpydc, linkers hosting Pd^{II} ions. The resulting material exhibited high crystallinity and thermal stability up to 400 °C, i.e. almost as remarkable than that of the not functionalized UiO-67 MOF.[38] Reduction of Pd^{II} to Pd^0 during H_2-TPR was monitored by simultaneous *in situ* XAS and XRPD and indicated the detachment of Pd^{II} ions from the linkers, removal of Cl^- ligands and growth of Pd NPs accompanied by the decrease of UiO-67 lattice parameter. The resulting material contained homogeneously distributed Pd particles with an average size of 2.1 nm. We showed that these small palladium NPs in MOF absorb less hydrogen in comparison with bigger carbon-supported palladium NPs, which is proved by smaller increase of Pd-Pd distances and less pronounces XANES features of the palladium hydride phase. Pd NPs in UiO-67 were catalytically active. IR and MS data showed high activity of the sample towards ethylene hydrogenation. In a mixture of hydrogen and ethylene, formation of palladium carbide was detected by difference XANES. Further growth of carbide features was observed in pure ethylene. The fact that carbide formation does not increase the Pd-Pd interatomic distances indicated that Pd-C bonds were formed only at the surface of the NPs.

Conflicts of interest

Authors declare no conflicts of interest.

Acknowledgments

A.L.B., A.A.G., M.A.S., A.V.S., and C.L. acknowledge Grant of the Southern Federal University (VnGr-07/2017-08). G.K., S.Ø.Ø., A.L., U.O. and K.-P.L. acknowledge the Norwegian Research Council for financial support through contract no. 250795. We are thankful to Vladimir Dmitriev, Herman Emerich, Wouter van Beek, and Michela Brunelli for their friendly and competent support during the experiment performed at the BM31 beamline of the ESRF. Suresh Gatla is kindly acknowledged for the support during the XAS experiment at the BM23 beamline of the ESRF. Koen Bossers, Cesare Atzori, Bjørn Tore Lønstad Bleken, and Boris Bouchevreau are also acknowledged for the help during the experiments.

Notes and references

1 G. Ferey, *Chem. Mater.*, 2001, **13**, 3084-3098.
2 J. J. Perry, J. A. Perman and M. J. Zaworotko, *Chem. Soc. Rev.*, 2009, **38**, 1400-1417.
3 D. J. Tranchemontagne, J. L. Mendoza-Cortes, M. O'Keeffe and O. M. Yaghi, *Chem. Soc. Rev.*, 2009, **38**, 1257-1283.
4 D. Zhao, D. J. Timmons, D. Q. Yuan and H. C. Zhou, *Acc. Chem. Res.*, 2011, **44**, 123-133.
5 M. O'Keeffe and O. M. Yaghi, *Chem. Rev.*, 2012, **112**, 675-702.
6 N. Stock and S. Biswas, *Chem. Rev.*, 2012, **112**, 933-969.
7 T. R. Cook, Y. R. Zheng and P. J. Stang, *Chem. Rev.*, 2013, **113**, 734-777.
8 H. Furukawa, K. E. Cordova, M. O'Keeffe and O. M. Yaghi, *Science*, 2013, **341**, 1230444.
9 V. V. Butova, M. A. Soldatov, A. A. Guda, K. A. Lomachenko and C. Lamberti, *Russ. Chem. Rev.*, 2016, **85**, 280-307.
10 Y. J. Cui, B. Li, H. J. He, W. Zhou, B. L. Chen and G. D. Qian, *Acc. Chem. Res.*, 2016, **49**, 483-493.
11 A. Schoedel, M. Li, D. Li, M. O'Keeffe and O. M. Yaghi, *Chem. Rev.*, 2016, **116**, 12466-12535.
12 T. L. Easun, F. Moreau, Y. Yan, S. H. Yang and M. Schroder, *Chem. Soc. Rev.*, 2017, **46**, 239-274.
13 Q. G. Zhai, X. H. Bu, X. Zhao, D. S. Li and P. Y. Feng, *Acc. Chem. Res.*, 2017, **50**, 407-417.

14 A. J. Howarth, A. W. Peters, N. A. Vermeulen, T. C. Wang, J. T. Hupp and O. K. Farha, *Chem. Mater.*, 2017, **29**, 26-39.
15 R. E. Morris and L. Brammer, *Chem. Soc. Rev.*, 2017, **46**, 5444-5462.
16 S. Øien-Odegaard, G. C. Shearer, D. S. Wragg and K. P. Lillerud, *Chem. Soc. Rev.*, 2017, **46**, 4867-4876.
17 J. W. Ren, M. Ledwaba, N. M. Musyoka, H. W. Langan, M. Mathe, S. J. Liao and W. Pang, *Coord. Chem. Rev.*, 2017, **349**, 169-197.
18 M. Bosch, S. Yuan, W. Rutledge and H. C. Zhou, *Acc. Chem. Res.*, 2017, **50**, 857-865.
19 S. L. Qiu and G. S. Zhu, *Coord. Chem. Rev.*, 2009, **253**, 2891-2911.
20 Z. Wang and S. M. Cohen, *Chem. Soc. Rev.*, 2009, **38**, 1315-1329.
21 H. X. Deng, C. J. Doonan, H. Furukawa, R. B. Ferreira, J. Towne, C. B. Knobler, B. Wang and O. M. Yaghi, *Science*, 2010, **327**, 846-850.
22 B. L. Chen, S. C. Xiang and G. D. Qian, *Acc. Chem. Res.*, 2010, **43**, 1115-1124.
23 K. K. Tanabe and S. M. Cohen, *Chem. Soc. Rev.*, 2011, **40**, 498-519.
24 S. M. Cohen, *Chem. Rev.*, 2012, **112**, 970-1000.
25 F. Llabrés i Xamena and J. Gascon, *Metal Organic Frameworks as Heterogeneous Catalysts*, Royal Society of Chemistry, Cambridge, 2013.
26 J. E. Mondloch, O. K. Farha and J. T. Hupp, in *Metal organic frameworks as heterogeneous catalysts*, eds. F. Llabrés i Xamena and J. Gascon, The Royal Society of Chemistry, Cambridge, 2013, ch. 9, pp. 289-309.
27 A. D. Burrows, in *Metal Organic Frameworks as Heterogeneous Catalysts*, eds. F. Llabrés i Xamena and J. Gascon, The Royal Society of Chemistry, Cambridge, 2013, pp. 31-75.
28 P. Deria, J. E. Mondloch, O. Karagiaridi, W. Bury, J. T. Hupp and O. K. Farha, *Chem. Soc. Rev.*, 2014, **43**, 5896-5912.
29 J. D. Evans, C. J. Sumby and C. J. Doonan, *Chem. Soc. Rev.*, 2014, **43**, 5933-5951.
30 W. G. Lu, Z. W. Wei, Z. Y. Gu, T. F. Liu, J. Park, J. Park, J. Tian, M. W. Zhang, Q. Zhang, T. Gentle, M. Bosch and H. C. Zhou, *Chem. Soc. Rev.*, 2014, **43**, 5561-5593.
31 Y. B. Huang, J. Liang, X. S. Wang and R. Cao, *Chem. Soc. Rev.*, 2017, **46**, 126-157.
32 T. Islamoglu, S. Goswami, Z. Y. Li, A. J. Howarth, O. K. Farha and J. T. Hupp, *Acc. Chem. Res.*, 2017, **50**, 805-813.
33 W. P. Lustig, S. Mukherjee, N. D. Rudd, A. V. Desai, J. Li and S. K. Ghosh, *Chem. Soc. Rev.*, 2017, **46**, 3242-3285.
34 M. Taddei, *Coord. Chem. Rev.*, 2017, **343**, 1-24.
35 Q. H. Yang, Q. Xu and H. L. Jiang, *Chem. Soc. Rev.*, 2017, **46**, 4774-4808.
36 J. H. Cavka, S. Jakobsen, U. Olsbye, N. Guillou, C. Lamberti, S. Bordiga and K. P. Lillerud, *J. Am. Chem. Soc.*, 2008, **130**, 13850-13851.
37 L. Valenzano, B. Civalleri, S. Chavan, S. Bordiga, M. H. Nilsen, S. Jakobsen, K. P. Lillerud and C. Lamberti, *Chem. Mater.*, 2011, **23**, 1700-1718.
38 S. Chavan, J. G. Vitillo, D. Gianolio, O. Zavorotynska, B. Civalleri, S. Jakobsen, M. H. Nilsen, L. Valenzano, C. Lamberti, K. P. Lillerud and S. Bordiga, *Phys. Chem. Chem. Phys.*, 2012, **14**, 1614-1626.
39 S. Øien, D. Wragg, H. Reinsch, S. Svelle, S. Bordiga, C. Lamberti and K. P. Lillerud, *Cryst. Growth Des.*, 2014, **14**, 5370-5372.
40 G. C. Shearer, S. Chavan, J. Ethiraj, J. G. Vitillo, S. Svelle, U. Olsbye, C. Lamberti, S. Bordiga and K. P. Lillerud, *Chem. Mater.*, 2014, **26**, 4068-4071.
41 G. C. Shearer, S. Chavan, S. Bordiga, S. Svelle, U. Olsbye and K. P. Lillerud, *Chem. Mater.*, 2016, **28**, 3749-3761.
42 G. C. Shearer, J. G. Vitillo, S. Bordiga, S. Svelle, U. Olsbye and K. P. Lillerud, *Chem. Mater.*, 2016, **28**, 7190-7193.
43 C. A. Trickett, K. J. Gagnon, S. Lee, F. Gandara, H. B. Burgi and O. M. Yaghi, *Angew. Chem. Int. Edit.*, 2015, **54**, 11162-11167.
44 Y. Bai, Y. B. Dou, L. H. Xie, W. Rutledge, J. R. Li and H. C. Zhou, *Chem. Soc. Rev.*, 2016, **45**, 2327-2367.
45 M. G. Goesten, M. F. de Lange, A. I. Olivos-Suarez, A. V. Bavykina, P. Serra-Crespo, C. Krywka, F. M. Bickelhaupt, F. Kapteijn and J. Gascon, *Nat. Commun.*, 2016, **7**, Art. n. 11832.
46 C. Wang, Z. G. Xie, K. E. deKrafft and W. L. Lin, *J. Am. Chem. Soc.*, 2011, **133**, 13445-13454.
47 F. Vermoortele, B. Bueken, G. Le Bars, B. Van de Voorde, M. Vandichel, K. Houthoofd, A. Vimont, M. Daturi, M. Waroquier, V. Van Speybroeck, C. Kirschhock and D. E. De Vos, *J. Am. Chem. Soc.*, 2013, **135**, 11465-11468.
48 H. H. Fei and S. M. Cohen, *Chem. Commun.*, 2014, **50**, 4810-4812.
49 M. Lammert, M. T. Wharmby, S. Smolders, B. Bueken, A. Lieb, K. A. Lomachenko, D. De Vos and N. Stock, *Chem. Commun.*, 2015, **51**, 12578-12581.
50 J. Hajek, M. Vandichel, B. Van de Voorde, B. Bueken, D. De Vos, M. Waroquier and V. Van Speybroeck, *J. Catal.*, 2015, **331**, 1-12.
51 D. Yang, S. O. Odoh, T. C. Wang, O. K. Farha, J. T. Hupp, C. J. Cramer, L. Gagliardi and B. C. Gates, *J. Am. Chem. Soc.*, 2015, **137**, 7391-7396.
52 I. Luz, C. Rosler, K. Epp, F. Xamena and R. A. Fischer, *Eur. J. Inorg. Chem.*, 2015, 3904-3912.

53 T. Toyao, K. Miyahara, M. Fujiwaki, T. H. Kim, S. Dohshi, Y. Horiuchi and M. Matsuoka, *J. Phys. Chem. C*, 2015, **119**, 8131-8137.
54 V. L. Rechac, F. G. Cirujano, A. Corma and F. Xamena, *Eur. J. Inorg. Chem.*, 2016, 4512-4516.
55 R. Dalapati, B. Sakthivel, A. Dhakshinamoorthy, A. Buragohain, A. Bhunia, C. Janiak and S. Biswas, *Crystengcomm*, 2016, **18**, 7855-7864.
56 P. Hester, S. J. Xu, W. Liang, N. Al-Janabi, R. Vakili, P. Hill, C. A. Muryn, X. B. Chen, P. A. Martin and X. L. Fan, *J. Catal.*, 2016, **340**, 85-94.
57 L. G. Ding, B. J. Yao, W. L. Jiang, J. T. Li, Q. J. Fu, Y. A. Li, Z. H. Liu, J. P. Ma and Y. B. Dong, *Inorg. Chem.*, 2017, **56**, 2337-2344.
58 E. S. Gutterød, S. Øien-Ødegaard, K. Bossers, A.-E. Nieuwelink, M. Manzoli, L. Braglia, A. Lazzarini, E. Borfecchia, S. Ahmadigoltapeh, B. Bouchevreau, B. T. Lønstad-Bleken, R. Henry, C. Lamberti, S. Bordiga, B. M. Weckhuysen, K. P. Lillerud and U. Olsbye, *Ind. Eng. Chem. Res.*, 2017, **56**, 13206-13218.
59 S. Smolders, K. A. Lomachenko, B. Bueken, A. Struyf, A. L. Bugaev, C. Atzori, N. Stock, C. Lamberti, M. B. J. Roeffaers and D. E. De Vos, *ChemPhysChem*, 2018, **19**, DOI: 10.1002/cphc.201700967.
60 T. Toyao, M. Saito, S. Dohshi, K. Mochizuki, M. Iwata, H. Higashimura, Y. Horiuchi and M. Matsuoka, *Res. Chem. Intermed.*, 2016, **42**, 7679-7688.
61 S. Øien-Ødegaard, B. Bouchevreau, K. Hylland, L. P. Wu, R. Blom, C. Grande, U. Olsbye, M. Tilset and K. P. Lillerud, *Inorg. Chem.*, 2016, **55**, 1986-1991.
62 M. Rimoldi, A. J. Howarth, M. R. DeStefano, L. Lin, S. Goswami, P. Li, J. T. Hupp and O. K. Farha, *ACS Catal.*, 2017, **7**, 997-1014.
63 H. Wu, Y. S. Chua, V. Krungleviciute, M. Tyagi, P. Chen, T. Yildirim and W. Zhou, *J. Am. Chem. Soc.*, 2013, **135**, 10525-10532.
64 L. Xu, Y. P. Luo, L. Sun, S. Pu, M. Fang, R. X. Yuan and H. B. Du, *Dalton Trans.*, 2016, **45**, 8614-8621.
65 S. Waitschat, D. Frohlich, H. Reinsch, H. Terraschke, K. A. Lomachenko, C. Lamberti, H. Kummer, T. Helling, M. Baumgartner, S. Henninger and N. Stock, *Dalton Trans.*, 2018, **48**, doi: 10.1039/C1037DT03641H.
66 D. D. Borges, S. Devautour-Vinot, H. Jobic, J. Ollivier, F. Nouar, R. Semino, T. Devic, C. Serre, F. Paesani and G. Maurin, *Angew. Chem. Int. Edit.*, 2016, **55**, 3919-3924.
67 D. D. Borges, R. Semino, S. Devautour-Vinott, H. Jobic, F. Paesani and G. Maurin, *Chem. Mater.*, 2017, **29**, 1569-1576.
68 G. W. Peterson, J. J. Mahle, J. B. DeCoste, W. O. Gordon and J. A. Rossin, *Angew. Chem. Int. Edit.*, 2016, **55**, 6235-6238.
69 C. H. Wang, X. L. Liu, J. P. Chen and K. Li, *Sci. Rep.*, 2015, **5**, 10.
70 Z. G. Hu, A. Nalaparaju, Y. W. Peng, J. W. Jiang and D. Zhao, *Inorg. Chem.*, 2016, **55**, 1134-1141.
71 A. Kronast, S. Eckstein, P. T. Altenbuchner, K. Hindelang, S. I. Vagin and B. Rieger, *Chem. Eur. J.*, 2016, **22**, 12800-12807.
72 S. Castarlenas, C. Tellez and J. Coronas, *J. Membr. Sci.*, 2017, **526**, 205-211.
73 I. Stassen, B. Bueken, H. Reinsch, J. F. M. Oudenhoven, D. Wouters, J. Hajek, V. Van Speybroeck, N. Stock, P. M. Vereecken, R. Van Schaijk, D. De Vos and R. Ameloot, *Chem. Sci.*, 2016, **7**, 5827-5832.
74 S. Jakobsen, D. Gianolio, D. S. Wragg, M. H. Nilsen, H. Emerich, S. Bordiga, C. Lamberti, U. Olsbye, M. Tilset and K. P. Lillerud, *Phys. Rev. B*, 2012, **86**, Art. n. 125429.
75 A. E. Platero-Prats, A. Mavrandonakis, L. C. Gallington, Y. Y. Liu, J. T. Hupp, O. K. Farha, C. J. Cramer and K. W. Chapmant, *J. Am. Chem. Soc.*, 2016, **138**, 4178-4185.
76 D. Yang, V. Bernales, T. Islamoglu, O. K. Farha, J. T. Hupp, C. J. Cramer, L. Gagliardi and B. C. Gates, *J. Am. Chem. Soc.*, 2016, **138**, 15189-15196.
77 C. Atzori, G. C. Shearer, L. Maschio, B. Civalleri, F. Bonino, C. Lamberti, S. Svelle, K. P. Lillerud and S. Bordiga, *J. Phys. Chem. C*, 2017, **121**, 9312-9324.
78 V. V. Butova, A. P. Budnyk, A. A. Guda, K. A. Lomachenko, A. L. Bugaev, A. V. Soldatov, S. M. Chavan, S. Øien-Ødegaard, U. Olsbye, K. P. Lillerud, C. Atzori, S. Bordiga and C. Lamberti, *Cryst. Growth Des.*, 2017, **17**, 5422-5431.
79 M. Kandiah, M. H. Nilsen, S. Usseglio, S. Jakobsen, U. Olsbye, M. Tilset, C. Larabi, E. A. Quadrelli, F. Bonino and K. P. Lillerud, *Chem. Mater.*, 2010, **22**, 6632-6640.
80 K. Lillerud, U. Olsbye and M. Tilset, *Top. Catal.*, 2010, **53**, 859-868.
81 S. J. Garibay and S. M. Cohen, *Chem. Commun.*, 2010, **46**, 7700-7702.
82 M. J. Katz, Z. J. Brown, Y. J. Colon, P. W. Siu, K. A. Scheidt, R. Q. Snurr, J. T. Hupp and O. K. Farha, *Chem. Commun.*, 2013, **49**, 9449-9451.
83 C. Kutzscher, G. Nickerl, I. Senkovska, V. Bon and S. Kaskel, *Chem. Mater.*, 2016, **28**, 2573-2580.
84 K. T. Hylland, S. Oien-Odegaard, K. P. Lillerud and M. Tilset, *Synlett*, 2015, **26**, 1480-1485.
85 N. C. Thacker, P. Ji, Z. Lin, A. Urban and W. Lin, *Faraday Discuss.*, 2017, **201**, 303-315.
86 M. I. Gonzalez, J. Oktawiec and J. R. Long, *Faraday Discuss.*, 2017, **201**, 351-367.
87 L. Braglia, E. Borfecchia, L. Maddalena, S. Øien, K. A. Lomachenko, A. L. Bugaev, S. Bordiga, A. V. Soldatov, K. P. Lillerud and C. Lamberti, *Catal. Today*, 2017, **283**, 89-103.

88 L. Braglia, E. Borfecchia, K. A. Lomachenko, A. L. Bugaev, A. A. Guda, A. V. Soldatov, B. T. L. Bleken, S. Oien, U. Olsbye, K. P. Lillerud, S. Bordiga, G. Agostini, M. Manzoli and C. Lamberti, *Faraday Discuss.*, 2017, **201**, 265-286.
89 C. H. Hendon, J. Bonnefoy, E. A. Quadrelli, J. Canivet, M. B. Chambers, G. Rousse, A. Walsh, M. Fontecave and C. Mellot-Draznieks, *Chem. Eur. J.*, 2016, **22**, 3713-3718.
90 L. Braglia, E. Borfecchia, K. Lomachenko, S. Øien, K. Lillerud and C. Lamberti, *J. Phys. Conf. Ser.*, 2016, **712**, 012053.
91 S. Øien, G. Agostini, S. Svelle, E. Borfecchia, K. A. Lomachenko, L. Mino, E. Gallo, S. Bordiga, U. Olsbye, K. P. Lillerud and C. Lamberti, *Chem. Mater.*, 2015, **27**, 1042-1056.
92 E. Borfecchia, S. Øien, S. Svelle, L. Mino, L. Braglia, G. Agostini, E. Gallo, K. Lomachenko, S. Bordiga, A. Guda, S. M. A., A. V. Soldatov, U. Olsbye, K. P. Lillerud and C. Lamberti, *J. Phys. Conf. Ser.*, 2016, **712**, 012125.
93 L. Braglia, E. Borfecchia, A. Martini, A. L. Bugaev, A. V. Soldatov, S. Oien-Odegaard, B. T. Lonstad-Bleken, U. Olsbye, K. P. Lillerud, K. A. Lomachenko, G. Agostini, M. Manzoli and C. Lamberti, *Phys. Chem. Chem. Phys.*, 2017, **19**, 27489-27507.
94 L. Y. Chen, X. D. Chen, H. L. Liu, C. H. Bai and Y. W. Li, *J. Mater. Chem. A*, 2015, **3**, 15259-15264.
95 A. Schaate, P. Roy, A. Godt, J. Lippke, F. Waltz, M. Wiebcke and P. Behrens, *Chem. Eur. J.*, 2011, **17**, 6643-6651.
96 W. van Beek, O. V. Safonova, G. Wiker and H. Emerich, *Phase Transit.*, 2011, **84**, 726-732.
97 P. M. Abdala, O. V. Safonova, G. Wiker, W. van Beek, H. Emerich, J. A. van Bokhoven, J. Sa, J. Szlachetko and M. Nachtegaal, *Chimia*, 2012, **66**, 699-705.
98 A. L. Bugaev, A. A. Guda, A. Lazzarini, K. A. Lomachenko, E. Groppo, R. Pellegrini, A. Piovano, H. Emerich, A. V. Soldatov, L. A. Bugaev, V. P. Dmitriev, J. A. van Bokhoven and C. Lamberti, *Catal. Today*, 2017, **283**, 119-126.
99 A. L. Bugaev, A. A. Guda, K. A. Lomachenko, V. V. Shapovalov, A. Lazzarini, J. G. Vitillo, L. A. Bugaev, E. Groppo, R. Pellegrini, A. V. Soldatov, J. A. van Bokhoven and C. Lamberti, *J. Phys. Chem. C*, 2017, **121**, 18202-18213.
100 C. W. Andersen, E. Borfecchia, M. Bremholm, M. R. V. Jorgensen, P. N. R. Vennestrom, C. Lamberti, L. F. Lundegaard and B. B. Iversen, *Angew. Chem. Int. Edit.*, 2017, **56**, 10367-10372.
101 C. Lamberti, S. Bordiga, F. Bonino, C. Prestipino, G. Berlier, L. Capello, F. D'Acapito, F. Xamena and A. Zecchina, *Phys. Chem. Chem. Phys.*, 2003, **5**, 4502-4509.
102 B. Ravel and M. Newville, *J. Synchrotron Radiat.*, 2005, **12**, 537-541.
103 D. C. Koningsberger, in *Neutron and synchrotron radiation for condensed matter studies. Applications to solid state physics and chemistry*, eds. J. Baruchel, J.-L. Hodeau, M. S. Lehmann, J.-R. Regnard and C. Schlenker, Springer, Berlin, 1994, pp. 213-244.
104 V. V. Srabionyan, A. L. Bugaev, V. V. Pryadchenko, L. A. Avakyan, J. A. Van Bokhoven and L. A. Bugaev, *J. Phys. Chem. Solids*, 2014, **75**, 470-476.
105 V. Petříček, M. Dušek and L. Palatinus, *Z. Kristallog.*, 2014, **229**, 345-352.
106 A. L. Bugaev, A. A. Guda, K. A. Lomachenko, V. V. Srabionyan, L. A. Bugaev, A. V. Soldatov, C. Lamberti, V. P. Dmitriev and J. A. van Bokhoven, *J. Phys. Chem. C*, 2014, **118**, 10416-10423.
107 M. Milanesio, G. Artioli, A. F. Gualtieri, L. Palin and C. Lamberti, *J. Am. Chem. Soc.*, 2003, **125**, 14549-14558.
108 G. Agostini, C. Lamberti, L. Palin, M. Milanesio, N. Danilina, B. Xu, M. Janousch and J. A. van Bokhoven, *J. Am. Chem. Soc.*, 2010, **132**, 667-678.
109 A. Piovano, G. Agostini, A. I. Frenkel, T. Bertier, C. Prestipino, M. Ceretti, W. Paulus and C. Lamberti, *J. Phys. Chem. C*, 2011, **115**, 1311-1322.
110 A. Martini, E. Borfecchia, K. A. Lomachenko, I. A. Pankin, C. Negri, G. Berlier, P. Beato, H. Falsig, S. Bordiga and C. Lamberti, *Chem. Sci.*, 2017, **8**, 6836-6851.
111 D. K. Pappas, E. Borfecchia, M. Dyballa, I. A. Pankin, K. A. Lomachenko, A. Martini, M. Signorile, S. Teketel, B. Arstad, G. Berlier, C. Lamberti, S. Bordiga, U. Olsbye, K. P. Lillerud, S. Svelle and P. Beato, *J. Am. Chem. Soc.*, 2017, **139**, 14961-14975.
112 A. I. Frenkel, *J. Synchrotron Radiat.*, 1999, **6**, 293-295.
113 S. Calvin, M. M. Miller, R. Goswami, S. F. Cheng, S. P. Mulvaney, L. J. Whitman and V. G. Harris, *J. Appl. Phys.*, 2003, **94**, 778-783.
114 G. Agostini, R. Pellegrini, G. Leofanti, L. Bertinetti, S. Bertarione, E. Groppo, A. Zecchina and C. Lamberti, *J. Phys. Chem. C*, 2009, **113**, 10485-10492.
115 G. Agostini, A. Piovano, L. Bertinetti, R. Pellegrini, G. Leofanti, E. Groppo and C. Lamberti, *J. Phys. Chem. C*, 2014, **118**, 4085-4094.
116 A. Borodzinki, *Catal. Rev. Sci. Eng.*, 2006, **48**, 91-144.
117 A. L. Bugaev, O. A. Usoltsev, A. Lazzarini, K. A. Lomachenko, A. A. Guda, R. Pellegrini, M. Carosso, J. G. Vitillo, E. Groppo, J. van Bokhoven, A. V. Soldatov and C. Lamberti, *Faraday Discussions*, 2018, DOI: 10.1039/c7fd00211d.
118 A. L. Bugaev, A. A. Guda, K. A. Lomachenko, A. Lazzarini, V. V. Srabionyan, J. G. Vitillo, A. Piovano, E. Groppo, L. A. Bugaev, A. V. Soldatov, V. P. Dmitriev, R. Pellegrini, J. A. van Bokhoven and C. Lamberti, *J. Phys. Conf. Ser.*, 2016, **712**, Art. n. 012032.
119 A. L. Bugaev, V. V. Srabionyan, A. V. Soldatov, L. A. Bugaev and J. A. van Bokhoven, *J. Phys. Conf. Ser.*, 2013, **430**, Art. n. 012028.

120 C. Lamberti, E. Groppo, G. Spoto, S. Bordiga and A. Zecchina, in *Advances in Catalysis, Vol 51*, eds. B. C. Gates and H. Knozinger, Elsevier Academic Press Inc, San Diego, 2007, vol. 51, pp. 1-74.
121 C. Lamberti, A. Zecchina, E. Groppo and S. Bordiga, *Chem. Soc. Rev.*, 2010, **39**, 4951-5001.
122 S. Bordiga, C. Lamberti, F. Bonino, A. Travert and F. Thibault-Starzyk, *Chem. Soc. Rev.*, 2015, **44**, 7262-7341.
123 F. Bonino, C. Lamberti, S. Chavan, J. G. Vitillo and S. Bordiga, in *Metal Organic Frameworks as Heterogeneous Catalysts*, eds. F. Llabrés i Xamena and J. Gascon, Royal Society of Chemistry, Cambridge, 2013, pp. 76-142.
124 G. C. Shearer, S. Forselv, S. Chavan, S. Bordiga, K. Mathisen, M. Bjorgen, S. Svelle and K. P. Lillerud, *Top. Catal.*, 2013, **56**, 770-782.
125 A. Brock, N. Minacamilde and C. Manzanares, *J. Phys. Chem.*, 1994, **98**, 4800-4808.

Table of contents image.

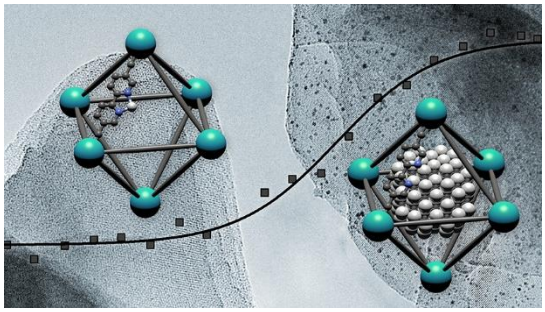

Formation of Pd nanoparticles inside UiO-67 MOF was monitored by *in situ* X-ray absorption and diffraction.